Computation of the Absorption Characteristics of a Two-Dimensional Rectangular Waveguide Array Using the Mode Matching Technique

A. Jöstingmeier, M. Dohlus and N. Holtkamp

Deutsches Elektronen-Synchrotron DESY
Gruppe Beschleunigerphysik
Notkestr. 85, D-22607 Hamburg, Germany

Abstract

It is planned to operate the TESLA linear collider with very short bunches leading to spectral components of the wakefield in the THz region. A special HOM (higher order modes) absorber similar to a two-dimensional array of rectangular waveguides has been proposed in order to couple out the wakefield from the accelerating structure. In this contribution, a mode matching analysis of such a waveguide array is presented. In this approach, the diffracted field in the region above the absorber is represented by the so-called Rayleigh expansion whereas inside the waveguides the complete set of waveguide modes is assumed. The absorption characteristics of a typical structure is studied in detail up to a frequency of 2 THz. The validity of the presented analysis is confirmed by computations carried out by the electromagnetic field simulator MAFIA.

I. Introduction

For the FEL operation mode of TESLA [1], very short bunches ($\sigma = 25\,\mu$m) are to be used. These bunches excite wakefields at the cavities and at other discontinuities in the vacuum chamber of the accelerator with spectral components up to the THz region ($f_{\max} \propto c_0/2\pi\sigma$, where c_0 denotes the velocity of light in vacuum). Frequencies above 700 GHz are especially undesirable because these spectral components can crack the Cooper pairs and lead to a significant reduction of the quality factor of the superconducting cavities and consequently to an excessive energy deposition in the 2 K cooling circuit.

In a typical refrigerator 800 W of wall plug power per Watt dissipated at 2 K are required [2]. The average power deposition due to wakefields is about 25 W per module [1]. Assuming that this power is completely absorbed at the 2 K level, which leads to a power consumption of the cooling system of about 20 kW per module, it is obvious that the wakefields must be extracted somewhere else at a higher temperature where the efficiency of the refrigerator is much better.

In [3], the design of a HOM absorber, which is schematically shown in Fig. 1, has been proposed. It consists of an array of rectangular waveguides surrounding the beam pipe between two succeeding cryogenic modules. With the help of this waveguide array, the high frequency components of the wakefields are efficiently extracted from the accelerating structure; whereas the low frequency part of the spectrum cannot significantly penetrate into the absorber waveguides. The propagating rectangular waveguide modes are then strongly attenuated by wall

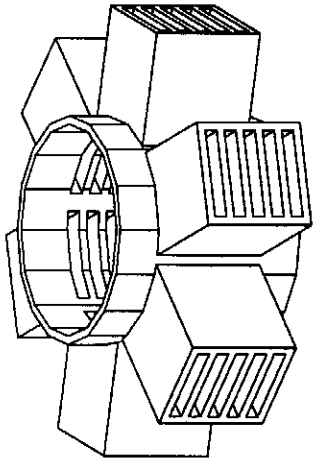

Figure 1: Schematic drawing of a HOM absorber.

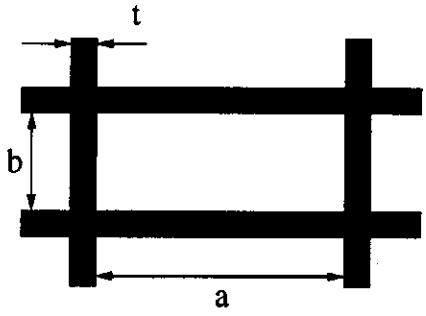

Figure 2: Waveguide dimensions.

losses being considerably high at frequencies above the cutoff frequency of the fundamental waveguide mode.

The absorber works at the same temperature level as the shield cooling which is 70 K. In this case the absorbed power has to be multiplied only by a factor of 25 yielding 625 W wall plug power per module for the cooling which is tolerable [2].

The waveguide dimensions which are defined in Fig. 2 are determined by the cutoff frequency of the absorber and the required attenuation of the waveguide modes. If the cutoff frequency is assumed to be 100 GHz, the width a of the rectangular waveguides has to be 1.5 mm.

The diameter of the absorber has to be less than 300 mm due to the limited space for its installation; and the diameter of the beampipe is 70 mm. Consequently, the length of the rectangular waveguides is less than 115 mm which means that a relatively high attenuation of the waveguide modes is necessary in order to guarantee that not too much power is reflected back into the beampipe. Fig. 3 shows the attenuation characteristics of the fundamental rectangular waveguide mode for various aspect ratios $a : b$ assuming that the waveguide is made of stainless steel with a conductivity of $0.5 \cdot 10^7$ S/m. The results presented in this diagram indicate that the attenuation can be adjusted by the choice of the ratio $a : b$. If we choose an aspect ratio of 5 : 1, which corresponds to a waveguide height of 0.3 mm, the attenuation of the fundamental waveguide mode is always larger than 70 dB/m. Thus, even if we assume the worst case, i.e., the incoming wave is totally reflected at the outer radius of the absorber, the VSWR is still less than 1.4 which is acceptable.

It is obvious that for a good coupling between the accelerating structure and the absorber the thickness of the waveguide walls should be as small as possible. Therefore $t = 0.1$ mm is assumed which seems to be the lower limit of this dimension from the mechanical point of view.

For the sake of simplicity of the field theoretical analysis of the absorber, we consider instead of the original configuration a two-dimensional infinite planar grating which is schematically shown in Fig. 4. The absorption characteristics of this model are expected to be very close to those of the original absorber for the following reasons: For frequencies higher than the lower frequency limit of the absorber the free-space wavelength of the electromagnetic field is much shorter than the radius of the beampipe. Consequently, the curvature can be neglected and we may use a planar model instead of the circular structure.

Taking the above discussed dimensions into account, it becomes clear that Fig. 1 is somewhat misleading because not only a few but more than 130 waveguides surround the beampipe.

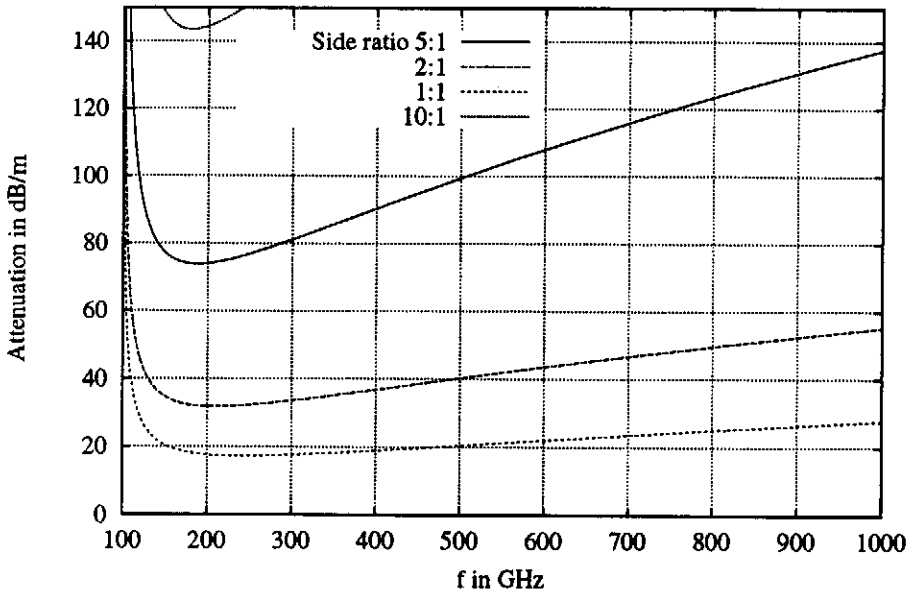

Figure 3: Attenuation of the fundamental mode corresponding to a rectangular waveguide made of stainless steel for various aspect ratios. Parameter: $a = 1.5\,\mathrm{mm}$, $\sigma = 0.5 \cdot 10^7\,\mathrm{S/m}$.

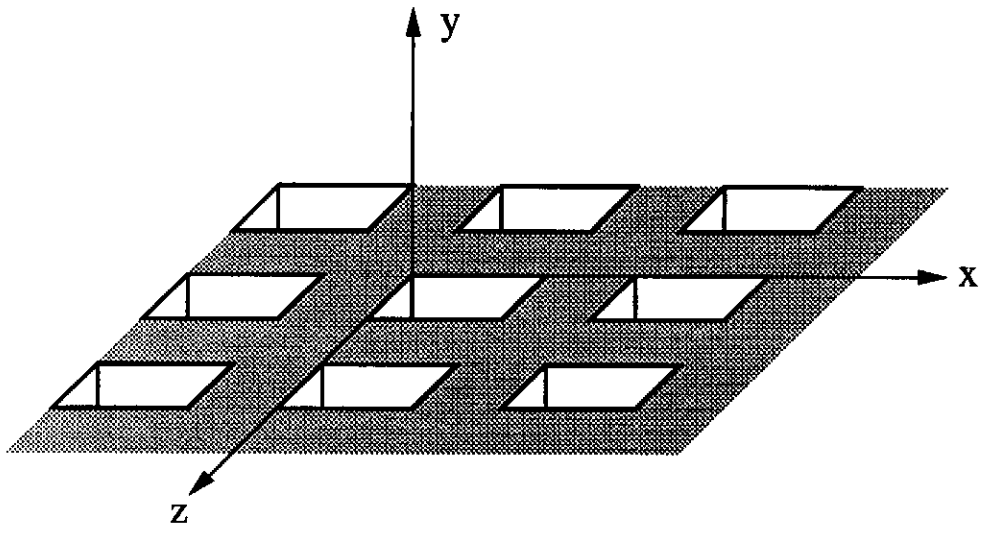

Figure 4: Schematic drawing of 3×3 cells of the grating.

Moreover, approximately 100 mm of space is availabe for the absorber in the axial direction. This means that about 250 layers of waveguides can be accomodated. Thus the absorber consists of a really large number of waveguides in both the axial and the azimuthal direction so that it may be approximated by an infinite grating with good accuracy.

Such a grating, which is none but a two-dimensional periodic structure, can be analyzed by the application of the mode matching technique. Above the grating the electromagnetic field is expanded in terms of an infinite series of spatial harmonics, which is known as the Rayleigh expansion. Inside the waveguides the electromagnetic field is represented by the complete spectrum of TE and TM waveguide modes. Matching the tangential electromagnetic field at either side of the waveguide aperture yields an infinite algebraic system of equations the unknown of which are the field expansion coefficients [4]–[6]. For the numerical solution one has to truncate the infinite system of equations. Therefore a detailed study of convergence is required in order to estimate the accuracy of the results.

The ratio describing how much of the power of the incoming wave is coupled into the waveguides is denoted as the grating efficiency. This ratio quantifies the power absorption properties of the structure. It is calculated for a grating with typical absorber dimensions in a broad frequency range and for various angles of incidence.

It will be shown that for the case of normal incidence of the incoming wave the field analysis of the waveguide array is equivalent to that of a step discontinuity in a waveguide. The validity of the presented method is then verified by comparing its results with those obtained by the electromagnetic field simulator MAFIA [7], [8] applied to a corresponding waveguide discontinuity.

II. Analysis

This section is devoted to the field theoretical analysis of the grating. It is organized as follows: The representations of the incident, the diffracted and the waveguide field are treated in Subsections IIa)–IIc). The matching of the aperture tangential field is then considered in Subsection IId). Finally, the required relations describing the condition of power conservation will be obtained in Subsection IIe).

IIa) The incident field

The parameters of the incident plane wave are defined in Fig. 5. The wavevector of this field is denoted by $\boldsymbol{k}$ so that with $\hat{\boldsymbol{k}}$ as unit vector along $\boldsymbol{k}$ and k_0 as free-space wave number we may write

$$\boldsymbol{k} = k_0 \hat{\boldsymbol{k}} \quad . \tag{1}$$

$\boldsymbol{k}$ can be decomposed into its cartesian components α_x, α_z and β:

$$\boldsymbol{k} = \hat{\boldsymbol{e}}_x \alpha_x + \hat{\boldsymbol{e}}_z \alpha_z - \hat{\boldsymbol{e}}_y \beta \quad , \tag{2}$$

where $\hat{e}_x$, $\hat{e}_y$ and $\hat{e}_z$ are unit vectors in x-, y-, and z-direction, respectively. Usually the wavevector is not given by its cartesian components but in terms of k_0 and the two angles Θ and ϑ which define the direction of incidence:

$$\alpha_x = \sin(\Theta)\cos(\vartheta)\, k_0 \quad , \tag{3}$$

$$\alpha_z = \sin(\Theta)\sin(\vartheta)\, k_0 \quad , \tag{4}$$

$$\beta = \cos(\Theta)\, k_0 \quad . \tag{5}$$

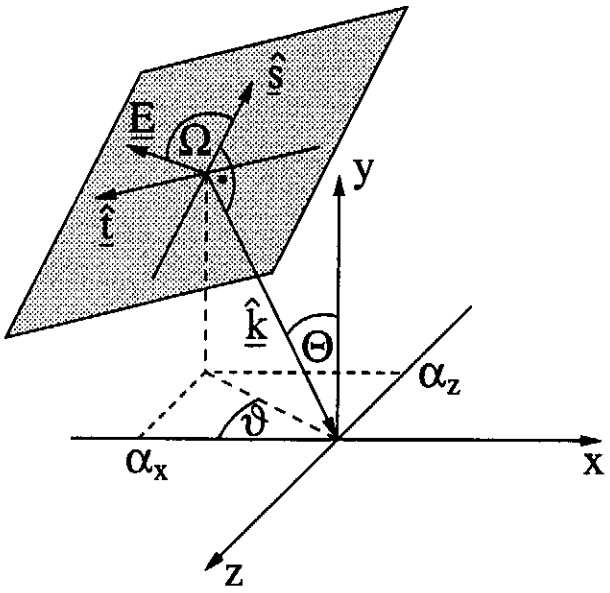

Figure 5: Definition of the angles and wavenumbers characterizing the incident wave.

For a complete description of the incident electromagnetic field, we need also further information about its amplitude and polarization. Let us assume that the incoming plane wave is linearly polarized. Then the electric field can uniquely be given by its amplitude E_0^i and the angle Ω:

$$\boldsymbol{E}^i = E_0^i \left(\cos(\Omega)\,\hat{\boldsymbol{s}} + \sin(\Omega)\,\hat{\boldsymbol{t}}\right) e^{-j(\alpha_x x + \alpha_z z - \beta y)} \quad , \tag{6}$$

where the unit vectors $\hat{\boldsymbol{s}}$ and $\hat{\boldsymbol{t}}$ define a plane normal to the wavevector. According to Fig. 5 the cartesian components of $\hat{\boldsymbol{s}}$ and $\hat{\boldsymbol{t}}$ read

$$\hat{\boldsymbol{s}} = \hat{\boldsymbol{e}}_x \cos(\vartheta)\cos(\Theta) + \hat{\boldsymbol{e}}_y \sin(\Theta) + \hat{\boldsymbol{e}}_z \sin(\vartheta)\cos(\Theta) \quad , \tag{7}$$

$$\hat{\boldsymbol{t}} = -\hat{\boldsymbol{e}}_x \sin(\vartheta) + \hat{\boldsymbol{e}}_z \cos(\vartheta) \quad . \tag{8}$$

For a plane wave the magnetic field $\boldsymbol{H}^i$ is related to the electric field by

$$\boldsymbol{H}^i = \frac{1}{Z_0}\left(\hat{\boldsymbol{k}} \times \boldsymbol{E}^i\right) \quad , \tag{9}$$

where Z_0 denotes the impedance of free space.

IIb) The diffracted field

The diffracted field can be decomposed into two partial fields. One of these fields is derived from an electric vector potential $\boldsymbol{F}$ and the other one from a magnetic vector potential $\boldsymbol{A}$ [9]. Each of the partial fields fulfils the source-free wave equation. Nevertheless the boundary condition at the grating interface ($y = 0$) can only be satisfied if both fields are taken into account.

The electric vector potential is defined as

$$\boldsymbol{E} = -\nabla \times \boldsymbol{F} \quad . \tag{10}$$

Due to the geometry of the structure it is convenient to use vector potentials directed along the y-coordinate which is perpendicular to the grating interface:

$$\boldsymbol{F} = \hat{\boldsymbol{e}}_y \Psi \tag{11}$$

Substituting Eqs. (10) and (11) into Maxwell's equations, it is found that the scalar potential Ψ is a solution of the homogeneous wave equation:

$$\boldsymbol{\nabla}^2 \Psi + k_0^2 \Psi = 0 \tag{12}$$

Finally the cartesian components of the partial field which is derived from the electric vector potential are

$$\boldsymbol{E} = \hat{\boldsymbol{e}}_x \frac{\partial}{\partial z}\Psi - \hat{\boldsymbol{e}}_z \frac{\partial}{\partial x}\Psi \quad , \tag{13}$$

$$\boldsymbol{H} = \frac{1}{jk_0 Z_0}\left(\hat{\boldsymbol{e}}_x \frac{\partial^2}{\partial x \partial y}\Psi + \hat{\boldsymbol{e}}_y \left(k_0^2 + \frac{\partial^2}{\partial y^2}\right)\Psi + \hat{\boldsymbol{e}}_z \frac{\partial^2}{\partial y \partial z}\Psi\right) \quad . \tag{14}$$

The magnetic vector potential $\boldsymbol{A}$ is usually defined without the minus sign of Eq. (10):

$$\boldsymbol{H} = \boldsymbol{\nabla} \times \boldsymbol{A} \tag{15}$$

The y-component of $\boldsymbol{A}$ is denoted by φ:

$$\boldsymbol{A} = \hat{\boldsymbol{e}}_y \varphi \tag{16}$$

Corresponding to Eq. (12), this scalar potential also fulfils the source-free wave equation

$$\boldsymbol{\nabla}^2 \varphi + k_0^2 \varphi = 0 \quad . \tag{17}$$

The electromagnetic field which is then derived from φ reads

$$\boldsymbol{E} = \frac{Z_0}{jk_0}\left(\hat{\boldsymbol{e}}_x \frac{\partial^2}{\partial x \partial y}\varphi + \hat{\boldsymbol{e}}_y \left(k_0^2 + \frac{\partial^2}{\partial y^2}\right)\varphi + \hat{\boldsymbol{e}}_z \frac{\partial^2}{\partial y \partial z}\varphi\right) \quad , \tag{18}$$

$$\boldsymbol{H} = -\hat{\boldsymbol{e}}_x \frac{\partial}{\partial z}\varphi + \hat{\boldsymbol{e}}_z \frac{\partial}{\partial x}\varphi \quad . \tag{19}$$

The Rayleigh expansion of the diffracted field is based on the fact that this field is pseudo-periodic (which means that it is periodic except for a phase factor) in the x- and the z-direction:

$$\varphi(x + L_x, y, z) = \varphi(x, y, z)\, e^{-j\alpha_x L_x} \quad , \tag{20}$$

$$\varphi(x, y, z + L_z) = \varphi(x, y, z)\, e^{-j\alpha_z L_z} \quad , \tag{21}$$

$$\Psi(x + L_x, y, z) = \Psi(x, y, z)\, e^{-j\alpha_x L_x} \quad , \tag{22}$$

$$\Psi(x, y, z + L_z) = \Psi(x, y, z)\, e^{-j\alpha_z L_z} \quad , \tag{23}$$

where L_x and L_z are the dimensions of one cell of the grating in the x- and the z-direction, respectively, which is illustrated in Fig. 6. Eqs. (20)–(23) mean that if we proceed a cell length $L_x(L_z)$ in the $x(z)$-direction the electromagnetic field is the same except for a phase factor of $e^{-j\alpha_x L_x}(e^{-j\alpha_z L_z})$ which is determined by the angle of incidence of the incoming wave. Thus,

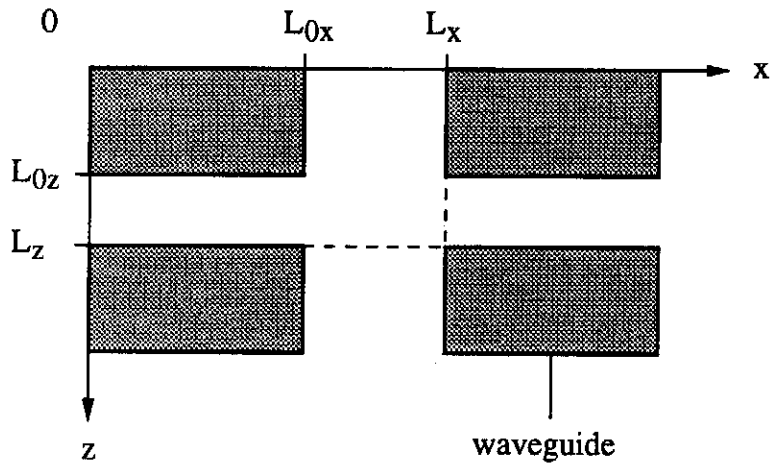

Figure 6: Definition of the grating dimensions.

we can expand these quantities into ordinary two-dimensional Fourier series if we multiply the potentials φ and Ψ by $e^{-j(\alpha_x x+\alpha_z z)}$:

$$\varphi(x,y,z) = \sum_{m,n=-\infty}^{\infty} B^A_{mn} e^{-j(\alpha_{xm}x+\alpha_{zn}z+\beta_{mn}y)} \quad , \tag{24}$$

$$\Psi(x,y,z) = \sum_{m,n=-\infty}^{\infty} B^F_{mn} e^{-j(\alpha_{xm}x+\alpha_{zn}z+\beta_{mn}y)} \tag{25}$$

The expansion coefficients of the spatial harmonics are denoted by B^A_{mn} and B^F_{mn}. The phase advance in the x- and the z-direction of the (m,n)th spatial harmonic is given by

$$\alpha_{xm} = \alpha_x - m\frac{2\pi}{L_x} \quad , \tag{26}$$

$$\alpha_{zn} = \alpha_z - n\frac{2\pi}{L_z} \tag{27}$$

respectively. Consequently the phase advance in the y-direction of the (m,n)th expansion term reads

$$\beta_{mn} = \begin{cases} \sqrt{k_0^2 - (\alpha_{xm}^2 + \alpha_{zn}^2)} & , \quad k_0^2 \geq \alpha_{xm}^2 + \alpha_{zn}^2 \\ -j\sqrt{(\alpha_{xm}^2 + \alpha_{zn}^2) - k_0^2} & , \quad k_0^2 < \alpha_{xm}^2 + \alpha_{zn}^2 \end{cases} . \tag{28}$$

The Rayleigh expansion means that for $y > 0$ the field can be represented by a series of outgoing plane waves having the same pseudo-periodicity as the incident field. It is worth noting that similar to waveguide modes only a finite number of plane waves are propagating upward whereas an infinite number of spatial harmonics constitute evanescent waves in the y-direction.

IIc) The waveguide field

Inside the rectangular waveguides the electromagnetic field is expanded in terms of the complete set of TE and TM modes with respect to the y-direction.

The cartesian components of the TE modes are

$$E_{xpq} = -A^H_{pq} N_{pq} k_{zq} \cos(k_{xp}x) \sin(k_{zq}z)\, e^{j\xi_{pq}y} \quad , \tag{29}$$

$$E_{zpq} = A^H_{pq} N_{pq} k_{xp} \sin(k_{xp}x) \cos(k_{zq}z)\, e^{j\xi_{pq}y} \quad , \tag{30}$$

$$E_{ypq} = 0 \quad , \tag{31}$$

$$H_{xpq} = -A^H_{pq} N_{pq} \frac{k_{xp}\xi_{pq}}{k_0 Z_0} \sin(k_{xp}x) \cos(k_{zq}z)\, e^{j\xi_{pq}y} \quad , \tag{32}$$

$$H_{zpq} = -A^H_{pq} N_{pq} \frac{k_{zq}\xi_{pq}}{k_0 Z_0} \cos(k_{xp}x) \sin(k_{zq}z)\, e^{j\xi_{pq}y} \quad , \tag{33}$$

$$H_{ypq} = A^H_{pq} N_{pq} \frac{k_{xp}^2 + k_{zq}^2}{jk_0 Z_0} \cos(k_{xp}x) \cos(k_{zq}z)\, e^{j\xi_{pq}y} \quad , \tag{34}$$

where Z_0 denotes the intrinsic impedance of free-space [10]. The normalizing quantity N_{pq} is given by

$$N_{pq} = \sqrt{\frac{1}{(1+\delta_{p0})(1+\delta_{q0})}} \quad , \tag{35}$$

where δ_{p0} is the Kronecker-delta. N_{pq} is introduced so that all TE modes including those with either $k_{xp} = 0$ or $k_{zq} = 0$ have the same length in functional space. The propagation factor ξ_{pq} reads

$$\xi_{pq} = \begin{cases} \sqrt{k_0^2 - \left(k_{xp}^2 + k_{zq}^2\right)} & , \quad k_0^2 \geq k_{xp}^2 + k_{zq}^2 \\ -j\sqrt{\left(k_{xp}^2 + k_{zq}^2\right) - k_0^2} & , \quad k_0^2 < k_{xp}^2 + k_{zq}^2 \end{cases} \quad \text{with} \tag{36}$$

$$k_{xp} = \frac{p\pi}{L_{0x}} \quad , \tag{37}$$

$$k_{zq} = \frac{q\pi}{L_{0z}} \quad ; \tag{38}$$

and A^H_{pq} denotes the amplitude of the (p,q)th TE mode.

For the cartesian components of the TM modes we can write

$$E_{xpq} = A^E_{pq} \frac{k_{xp}\xi_{pq} Z_0}{k_0} \cos(k_{xp}x) \sin(k_{zq}z)\, e^{j\xi_{pq}y} \quad , \tag{39}$$

$$E_{zpq} = A^E_{pq} \frac{k_{zq}\xi_{pq} Z_0}{k_0} \sin(k_{xp}x) \cos(k_{zq}z)\, e^{j\xi_{pq}y} \quad , \tag{40}$$

$$E_{ypq} = A^E_{pq} \frac{\left(k_{xp}^2 + k_{zq}^2\right) Z_0}{jk_0} \sin(k_{xp}x) \sin(k_{zq}z)\, e^{j\xi_{pq}y} \quad , \tag{41}$$

$$H_{xpq} = -A^E_{pq} k_{zq} \sin(k_{xp}x) \cos(k_{zq}z)\, e^{j\xi_{pq}y} \quad , \tag{42}$$

$$H_{zpq} = A^E_{pq} k_{xp} \cos(k_{xp}x) \sin(k_{zq}z)\, e^{j\xi_{pq}y} \quad , \tag{43}$$

$$H_{ypq} = 0 \quad . \tag{44}$$

The amplitude of the (p,q)th TM mode is denoted by A^E_{pq}. The propagation factor ξ_{pq} which is defined in Eq. (36) is valid for both TE and TM modes. On the other hand, a normalizing factor similar to N_{pq} is not required for TM modes because these modes do not exist for $k_{xp} = 0$ or $k_{zq} = 0$.

IId) Matching of the tangential fields in the aperture

In the preceding three Subsections IIa)–IIc) the incident, the diffracted and the waveguide field are considered which from now on are marked with a superscript i, r and w, respectively. In this subsection the corresponding fields are matched at the grating interface in order to obtain a linear system of equations for the still unknown field expansion coefficients B^A_{mn}, B^F_{mn}, A^H_{pq} and A^E_{pq}.

Matching the tangential electric field in the common aperture over one unit cell yields one equation for the x-component and another one for the z-component:

$$E^i_x\big|_{y=0} + E^r_x\big|_{y=0} = \begin{cases} E^w_x\big|_{y=0} & , \quad 0 < x < L_{0x} \quad \text{and} \quad 0 < z < L_{0z} \\ 0 & , \quad \text{otherwise} \end{cases} , \tag{45}$$

$$E^i_z\big|_{y=0} + E^r_z\big|_{y=0} = \begin{cases} E^w_z\big|_{y=0} & , \quad 0 < x < L_{0x} \quad \text{and} \quad 0 < z < L_{0z} \\ 0 & , \quad \text{otherwise} \end{cases} \tag{46}$$

After inserting the corresponding expansions for the incident, the diffracted and the waveguide field into Eqs. (45) and (46), multiplying both sides of the resulting equations by $e^{+j(\alpha_{xr}x+\alpha_{zs}z)}$ and integrating over one cell of the grating leads to two infinite sets of equations:

$$E^i_{0x}\delta_{r0}\delta_{s0} + j\left(-\alpha_{zs}B^F_{rs} + \frac{\alpha_{xr}\beta_{rs}}{k_0}\left(B^A_{rs}Z_0\right)\right) =$$

$$-\frac{L_{0x}L_{0z}}{L_xL_z}\left(\sum_{\substack{p=0\\q=1}}^{\infty} k_{zq}N_{pq}I^{xc}_{rp}I^{zs}_{sq}A^H_{pq} + \sum_{p,q=1}^{\infty}\frac{\xi_{pq}k_{xp}}{k_0}I^{xc}_{rp}I^{zs}_{sq}\left(A^E_{pq}Z_0\right)\right)$$

$$\text{for} \quad r,s = -\infty,\ldots,0,\ldots,\infty \quad , \tag{47}$$

$$E^i_{0z}\delta_{r0}\delta_{s0} + j\left(\alpha_{xr}B^F_{rs} + \frac{\alpha_{zs}\beta_{rs}}{k_0}\left(B^A_{rs}Z_0\right)\right) =$$

$$\frac{L_{0x}L_{0z}}{L_xL_z}\left(\sum_{\substack{p=1\\q=0}}^{\infty} k_{xp}N_{pq}I^{xs}_{rp}I^{zc}_{sq}A^H_{pq} + \sum_{p,q=1}^{\infty}\frac{\xi_{pq}k_{zq}}{k_0}I^{xs}_{rp}I^{zc}_{sq}\left(A^E_{pq}Z_0\right)\right)$$

$$\text{for} \quad r,s = -\infty,\ldots,0,\ldots,\infty \quad , \tag{48}$$

where E^i_{0x} and E^i_{0z} denote the x- and the z-component of the electric field amplitude of the incident wave, respectively. The quantities I^{xc}_{rp}, I^{zs}_{sq}, I^{xs}_{rp} and I^{zc}_{sq} are one-dimensional coupling integrals which measure the similarity between the pth(qth) waveguide eigenfunction and the rth(sth) spatial harmonic in the $x(z)$-direction:

$$I^{xc}_{rp} = \frac{1}{L_{0x}}\int_{x=0}^{L_{0x}} \cos(k_{xp}x)\,e^{j\alpha_{xr}x}dx \quad , \tag{49}$$

$$I^{zs}_{sq} = \frac{1}{L_{0z}}\int_{z=0}^{L_{0z}} \sin(k_{zq}z)\,e^{j\alpha_{zs}z}dz \quad , \tag{50}$$

$$I_{rp}^{xs} = \frac{1}{L_{0x}} \int_{x=0}^{L_{0x}} \sin(k_{xp}x)\, e^{j\alpha_{xr}x} dx \quad , \tag{51}$$

$$I_{sq}^{zc} = \frac{1}{L_{0z}} \int_{z=0}^{L_{0z}} \cos(k_{zq}z)\, e^{j\alpha_{zs}z} dz \tag{52}$$

These integrals can be evaluated analytically giving

$$I_{rp}^{xc} = \frac{j\alpha_{xr}L_{0x}}{(p\pi)^2 - (\alpha_{xr}L_{0x})^2} \left(e^{j\alpha_{xr}L_{0x}}(-1)^p - 1\right) \quad , \tag{53}$$

$$I_{sq}^{zs} = \frac{q\pi}{(q\pi)^2 - (\alpha_{zs}L_{0z})^2} \left(-e^{j\alpha_{zs}L_{0z}}(-1)^q + 1\right) \quad , \tag{54}$$

$$I_{rp}^{xs} = \frac{p\pi}{(p\pi)^2 - (\alpha_{xr}L_{0x})^2} \left(-e^{j\alpha_{xr}L_{0x}}(-1)^p + 1\right) \quad , \tag{55}$$

$$I_{sq}^{zc} = \frac{j\alpha_{zs}L_{0z}}{(q\pi)^2 - (\alpha_{zs}L_{0z})^2} \left(e^{j\alpha_{zs}L_{0z}}(-1)^q - 1\right) \quad . \tag{56}$$

The mode matching analysis of the grating results in a typical boundary reduction problem. This means that the x- and the z-components of the electric field above the grating must fulfil a boundary condition at the grating interface for all points in the xz-plane. On the other hand, the magnetic field has to satisfy the continuity conditions

$$H_z^i\big|_{y=0} + H_z^r|_{y=0} = H_z^w|_{y=0} \quad , \quad 0 < x < L_{0x} \quad \text{and} \quad 0 < z < L_{0z} \quad , \tag{57}$$

$$H_x^i\big|_{y=0} + H_x^r|_{y=0} = H_x^w|_{y=0} \quad , \quad 0 < x < L_{0x} \quad \text{and} \quad 0 < z < L_{0z} \tag{58}$$

only at the waveguide apertures. After inserting the appropriate field representations for H_z^i, H_z^r and H_z^w into Eq. (57), both sides of the resulting equation are then multiplied by $N_{uv}\sin\left(\frac{u\pi x}{L_{0x}}\right)\cos\left(\frac{v\pi z}{L_{0z}}\right)$ for $u = 1, 2, \ldots \infty$ and $v = 0, 1, \ldots \infty$ and integrated over the waveguide aperture yielding:

$$H_{0x}^i N_{uv} \left(I_{0u}^{xs}\right)^* \left(I_{0v}^{zc}\right)^* + j \sum_{m,n=-\infty}^{\infty} \left(\frac{\alpha_{xm}\beta_{mn}}{k_0} B_{mn}^F + \alpha_{zn}\left(B_{mn}^A Z_0\right)\right) N_{uv} \left(I_{mu}^{xs}\right)^* \left(I_{nv}^{zc}\right)^* =$$

$$\frac{1}{4}\left(-\frac{\xi_{uv}k_{xu}}{k_0} A_{uv}^H - k_{zv}\left(A_{uv}^E Z_0\right)\right) \quad \text{for} \quad u = 1, 2, \ldots \infty \quad , \quad v = 0, 1, \ldots \infty \tag{59}$$

The asterisk means complex conjugate; and H_{0x} is the x-component of the amplitude of the magnetic field corresponding to the incoming wave.

Correspondingly, Eq. (58) is multiplied by $N_{uv}\cos\left(\frac{u\pi x}{L_{0x}}\right)\sin\left(\frac{v\pi z}{L_{0z}}\right)$ for $u = 0, 1, \ldots \infty$ and $v = 1, 2, \ldots \infty$ and then integrated leading to

$$H_{0z}^i N_{uv} \left(I_{0u}^{xc}\right)^* \left(I_{0v}^{zs}\right)^* + j \sum_{m,n=-\infty}^{\infty} \left(\frac{\alpha_{zn}\beta_{mn}}{k_0} B_{mn}^F - \alpha_{xm}\left(B_{mn}^A Z_0\right)\right) N_{uv} \left(I_{mu}^{xc}\right)^* \left(I_{nv}^{zs}\right)^* =$$

$$\frac{1}{4}\left(-\frac{\xi_{uv}k_{zv}}{k_0} A_{uv}^H + k_{xu}\left(A_{uv}^E Z_0\right)\right) \quad \text{for} \quad u = 0, 1, \ldots \infty \quad , \quad v = 1, 2, \ldots \infty \quad . \tag{60}$$

The modal expansion coefficients B_{mn}^A, B_{mn}^F, A_{pq}^H and A_{pq}^E are now uniquely determined by solving the linear infinite system of equations which consists of Eqs. (47), (48), (59) and (60).

IIe) Power conservation

The grating is assumed to be lossless. Consequently, the sum of the power of the diffracted and the waveguide field is equal to the power of the incident wave:

$$P^i = P^r + P^w \tag{61}$$

This condition may be used in order to examine the correctness of our numerical results. Nevertheless, one has to bear in mind that Eq. (61) is satisfied for any number of field expansion terms. Therefore the condition of power conservation does not yield any information about the accuracy of the results.

The time-averaged power transmitted across the area of one grating cell by the incident wave is given by one-half of the real part of the integral of the $(-y)$-component of the complex Poynting vector $\boldsymbol{E}^i \times \left(\boldsymbol{H}^i\right)^*$:

$$P^i = \frac{1}{2}\mathrm{Re}\left\{\int_{x=0}^{L_x}\int_{z=0}^{L_z}\left(\boldsymbol{E}^i \times \left(\boldsymbol{H}^i\right)^*\right)\cdot(-\hat{\boldsymbol{e}}_y)\,dx\,dz\right\} \tag{62}$$

Inserting Eqs. (2), (5) and (9) into (62) yields

$$P^i = \frac{1}{2}L_x L_z \frac{|E_0^i|^2}{Z_0}\cos(\theta) \quad . \tag{63}$$

As expected, the power of the incident wave is proportional to the square of $|E_0^i|$ and to $\cos(\theta)$. The latter term is unity for a normal incident wave and vanishes for grazing incidence.

The power of the diffracted and the waveguide field can correspondingly be evaluated from

$$P^r = \frac{1}{2}\mathrm{Re}\left\{\int_{x=0}^{L_x}\int_{z=0}^{L_z}\left(-E_x^r\,(H_z^r)^* + E_z^r\,(H_x^r)^*\right)dx\,dz\right\} \quad , \tag{64}$$

$$P^w = \frac{1}{2}\mathrm{Re}\left\{\int_{x=0}^{L_x}\int_{z=0}^{L_z}\left(E_x^w\,(H_z^w)^* - E_z^w\,(H_x^w)^*\right)dx\,dz\right\} \quad , \tag{65}$$

respectively. If we replace the field components in Eqs. (64) and (65) by the corresponding series representations according to Eqs. (13), (14), (18), (19), (24) and (25) for the diffracted field and (29), (30), (32), (33), (39), (40), (42) and (43) for the waveguide field we finally arrive at

$$P^r = \frac{1}{2}\mathrm{Re}\left\{\frac{L_x L_z}{k_0}\sum_{m,n=-\infty}^{\infty}\left(\alpha_{xm}^2+\alpha_{zn}^2\right)\beta_{mn}\left(\left|B_{mn}^A\right|^2+\left|\frac{B_{mn}^F}{Z_0}\right|^2\right)\right\} , \tag{66}$$

$$P^w = \frac{1}{2}\mathrm{Re}\left\{\frac{L_{0x}L_{0z}}{4k_0 Z_0}\left(\sum_{\substack{p,q\geq 0\\ p+q>0}}^{\infty}\left(k_{xp}^2+k_{zq}^2\right)\xi_{pq}\left|A_{pq}^H\right|^2+\sum_{p,q\geq 1}^{\infty}\left(k_{xp}^2+k_{zq}^2\right)\xi_{pq}\left|A_{pq}^E Z_0\right|^2\right)\right\} . \tag{67}$$

Note that although the series of Eqs. (66) and (67) extend over all spatial harmonics and waveguide modes only those terms with a real β_{mn} and a real ξ_{pq} contribute to P^r and P^w, respectively.

The condition of power conservation is routinely monitored; and it is fulfilled for all numerical results which are presented in the next section.

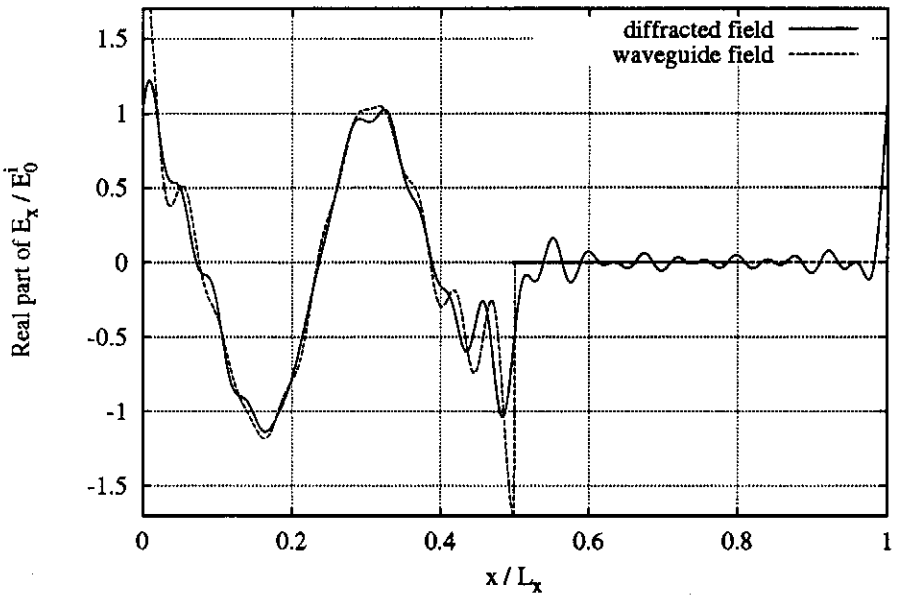

Figure 7: Real part of E_x/E_0^i along a line with $z = 0.02 \cdot L_x$. Parameters: $L_z = 0.2 \cdot L_x$, $L_{0x} = 0.5 \cdot L_x$, $L_{0z} = 0.1 \cdot L_x$, $\Theta = 0.5 \cdot \pi/2$, $\vartheta = 0.1 \cdot \pi/2$, $\Omega = 0$, $k_0 = 35/L_x$.

III. Numerical results

Let us start the discussion of the numerical results with a check of the validity of the presented method. According to Subsection IId) the aperture tangential components of the sum of the incident and the diffracted field must be equal to the corresponding waveguide field. Furthermore the x- and the z-component of the electric field at $y = 0$ have to vanish outside the waveguide aperture.

Figs. 7 and 8 show the real part of the x-component of the electric and the magnetic field strength, respectively, along a line with z = constant. These figures confirm that the field distributions at both sides of the waveguide aperture are indeed identical except for some small oscillations due to the well-known Gibb's phenomenon [11]. Moreover, E_x is very close to zero for $L_{0x} < x < L_x$ as it should be.

As already mentioned, we have to truncate the infinite system of equations for the practical implementation of the mode matching analysis. This limits the accuracy of the results which can, of course, be improved by taking more field expansion terms into account. On the other hand a higher number of expansion terms means that a larger system of equations has to be solved. Therefore one has to find a trade-off between the accuracy of the results and the required amount of computer resources.

In order to estimate the accuracy of the results, it is useful to study the convergence of the method with respect to the number of field expansion functions. Fig. 9 shows the grating efficiency as a function of the maximum order of the spatial harmonics in the x-direction N_x for a grating with typical dimensions of the proposed absorber: $a = 1.5\,\text{mm}$, $b = 0.3\,\text{mm}$ and $t = 0.1\,\text{mm}$. The normalized wavenumbers $k_0 L_x = 70$, 35, 17 and 7 correspond to frequencies of approximately 2000, 1000, 500 and 200 GHz, respectively.

For a frequency of 200 GHz accurate results are already obtained for $N_x = 5$. It is obvious that N_x has to be increased for higher frequencies. From Fig. 9 it can be concluded that for a

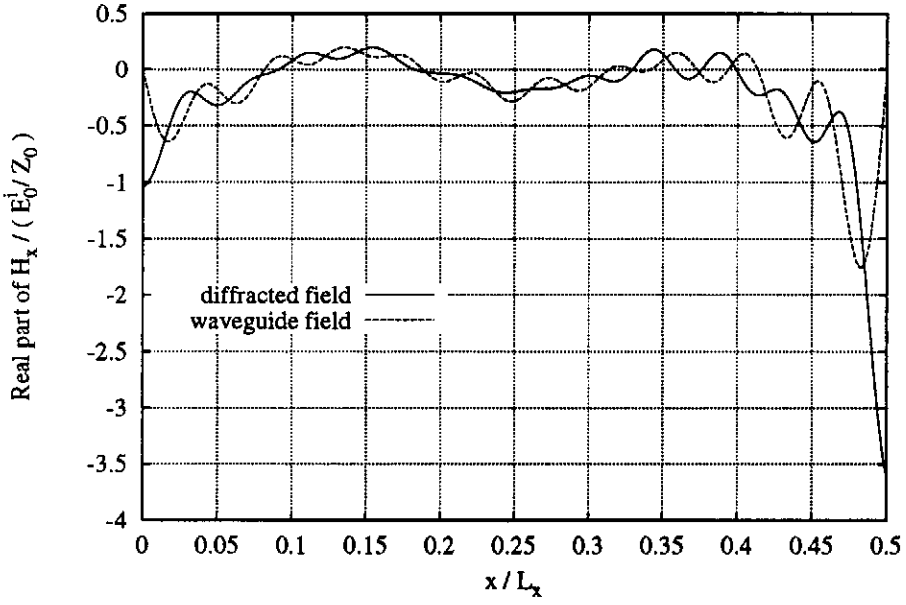

Figure 8: Real part of $H_x/(E_0^i/Z_0)$ along a line with $z = 0.02 \cdot L_x$. Parameters: see Fig. 7.

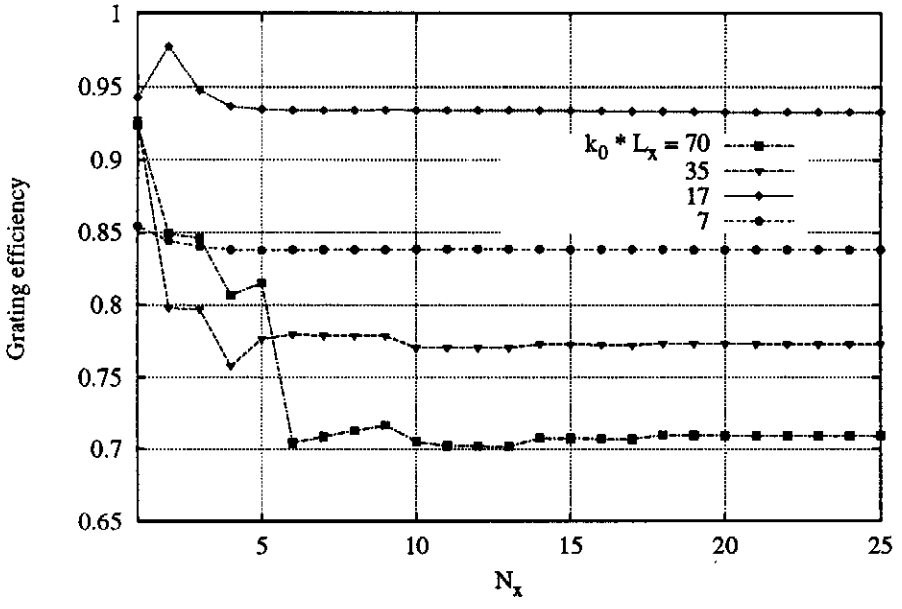

Figure 9: Grating efficiency as a function of the number of field expansion terms for various frequencies. Parameters: $L_z = 0.25 \cdot L_x$, $L_{0x} = 0.9375 \cdot L_x$, $L_{0z} = 0.1875 \cdot L_x$, $\Theta = 0$, $\vartheta = \pi/2$, $\Omega = 0$.

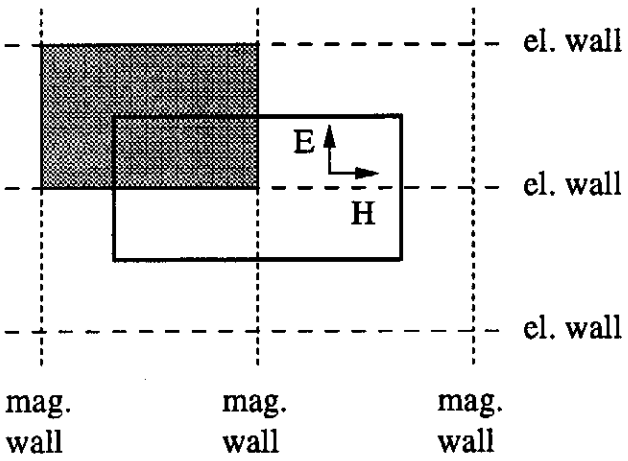

Figure 10: Reduction of the grating analysis to a waveguide discontinuity problem.

frequency of 2000 GHz $N_x = 20$ is sufficient. Thus this value is used for all further calculations. $N_x = 20$ means that approximately a (1500 × 1500) linear system of equations has to be solved. Assuming this parameter, a typical frequency scan with 1000 points requires about 2 d of cpu-time on a modern workstation, which is tolerable.

If the electric field vector of the incoming wave goes along the x- or the z-direction the analysis of the array of rectangular waveguides reduces to a simple waveguide discontinuity problem. This is illustrated in Fig. 10. Due to the periodicity of the structure in the x- and the z-direction, it is sufficient to consider a single cell of the grating which is bounded by perfect electric and magnetic walls normal to the electric and the magnetic field vectors, respectively. Keeping in mind that the electrically and magnetically conducting walls correspond to a short circuit and an open circuit, respectively, it becomes clear that the analysis of the grating is nothing else than a discontinuity problem between a parallel-plate and a rectangular waveguide. Furthermore we have two additional planes of symmetry for each cell dividing it into four identical pieces. Thus only one quarter of the waveguide discontinuity problem has actually to be considered as shown in Fig. 11.

Such a discontinuity is analyzed using the MAFIA computer code. The results are then used as a reference in order to check the validity of the presented mode matching technique.

It is worth noting that for the application of the mode matching technique instead of $\Theta = 0$ a very small angle Θ of approximately 1° is assumed because the case of a really normally incoming wave is not covered by the field representation of the diffracted field for the following reason: The diffracted field is derived from electric and magnetic vector potentials with respect to the y-direction. These vector potentials are proportional to the y-components of the electromagnetic field according to Eqs. (14) and (18) which are not present for a normal incident field. Thus, if a TEM field with respect to the y-direction is not taken into account explicitly, which is not the case, we have to assume a small angle Θ. Fig. 12 shows the excitation of the TE_{10}, the TE_{30} and the TE_{50} rectangular waveguide modes as result of both methods. It is found that in the investigated frequency range from 100 GHz to about 700 GHz the results agree very well.

The absorption characteristics for a normally incident, an obliquely incident and a nearly grazing incident field are presented in Figs. 13, 14 and 15, respectively. For a normally incident field the absorption characteristics is relatively well-behaved with the exception of some kinks which are observed at frequencies where either one of the spatial harmonics or one of the

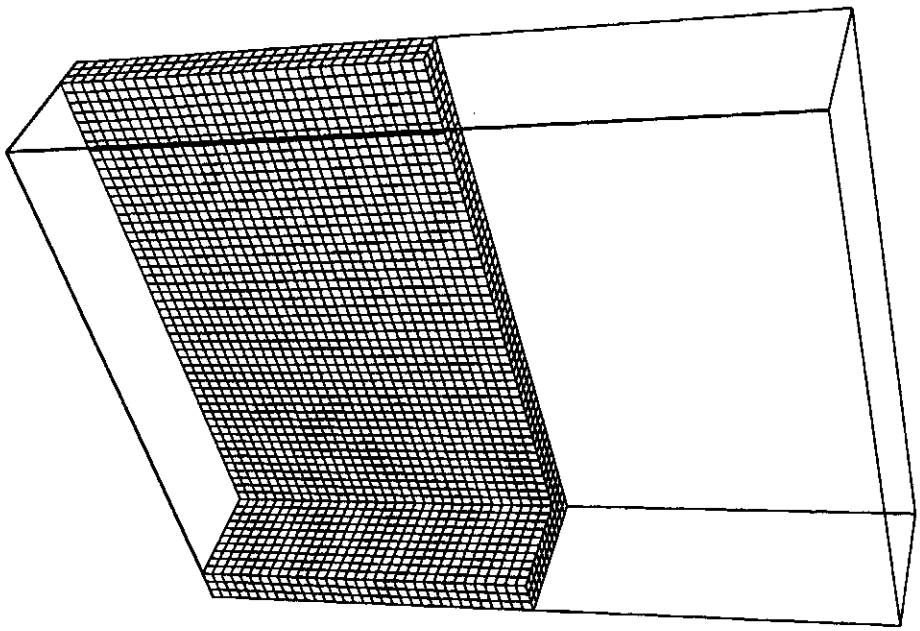

Figure 11: Three-dimensional view of one quarter of the discontinuity between a rectangular (L.H.S.) and a parallel-plate (R.H.S.) waveguide.

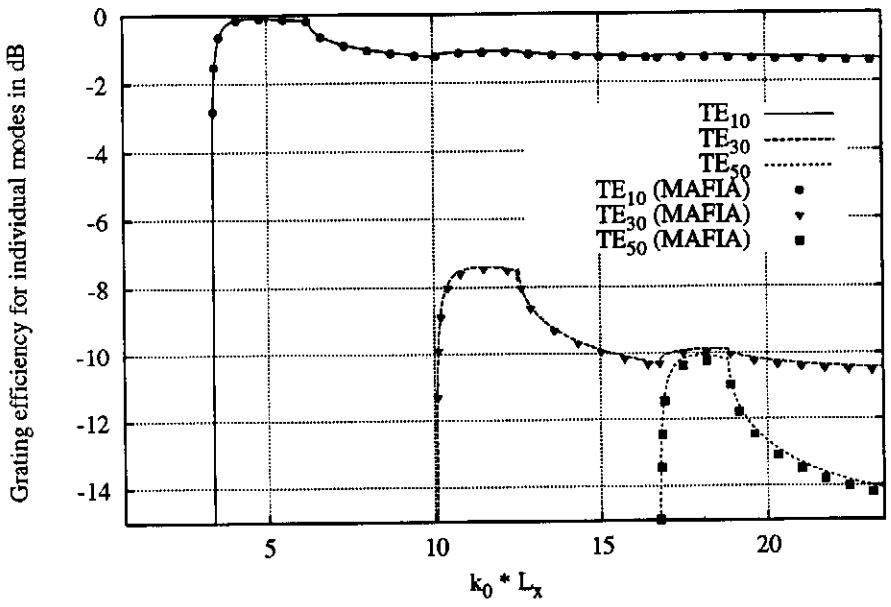

Figure 12: Comparison between the MAFIA computer code and the presented mode matching technique. Parameters: see Fig. 9.

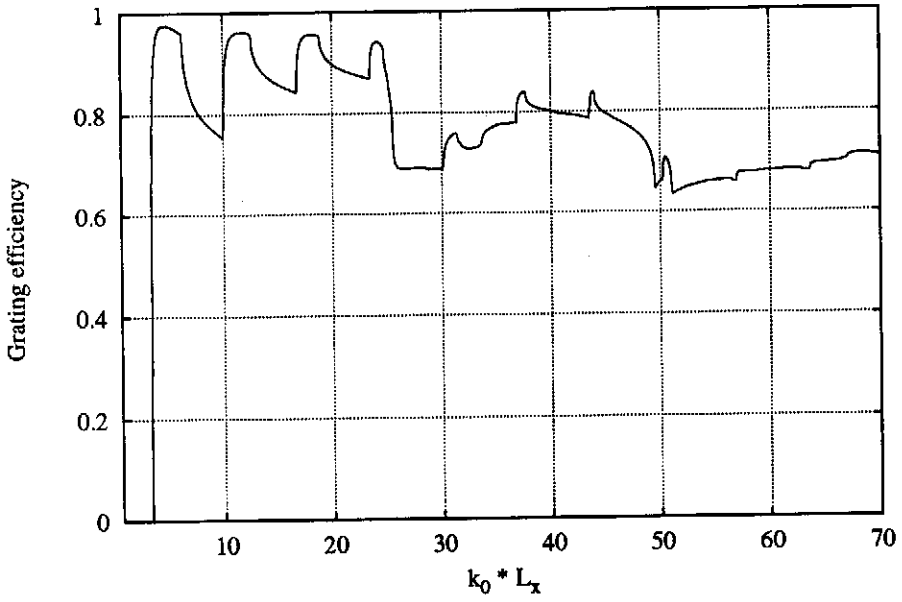

Figure 13: Absorption characteristics for a normally incident field. Other parameters: see Fig. 9.

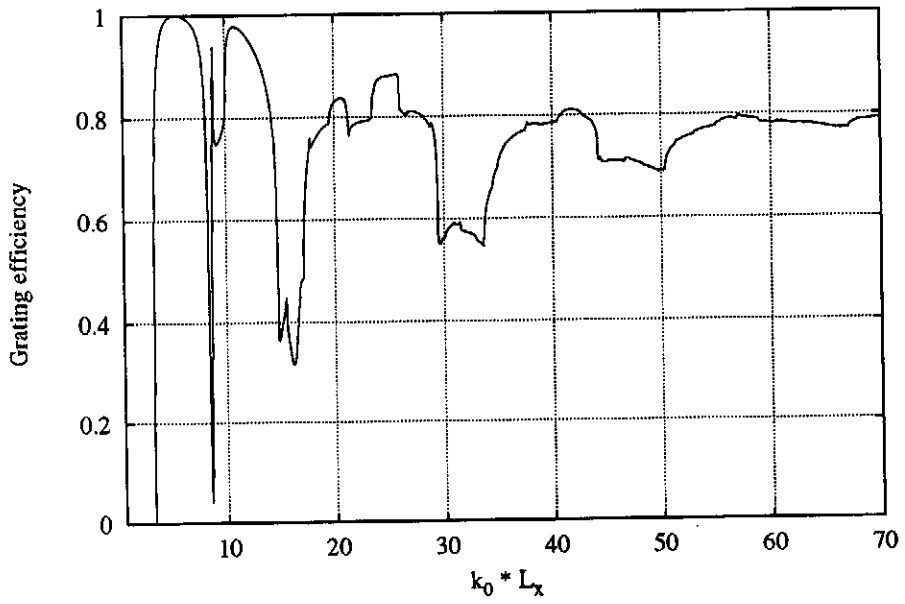

Figure 14: Absorption characteristics for an obliquely ($\Theta = 45°$) incident field. Other parameters: see Fig. 9.

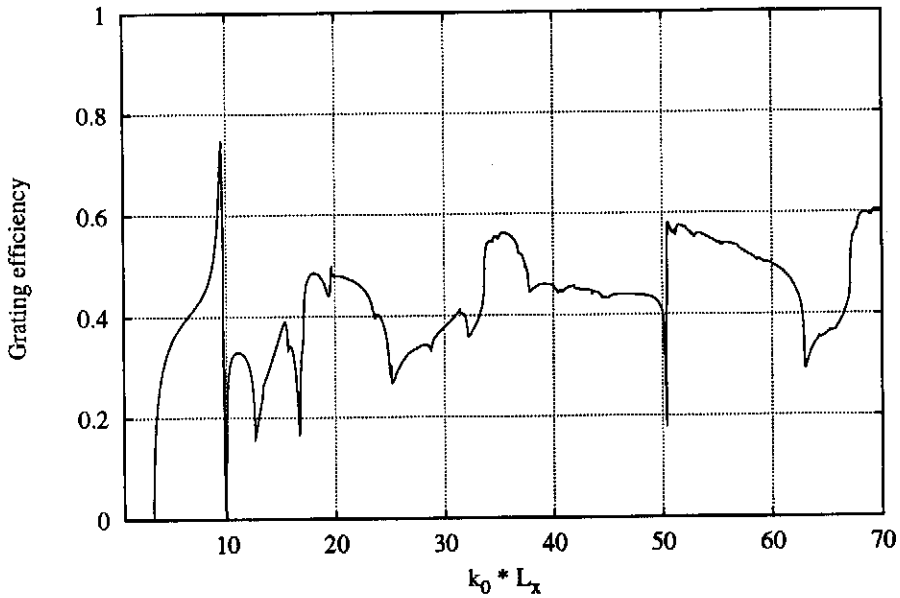

Figure 15: Absorption characteristics for a nearly grazing ($\Theta = 85.5°$) incident field. Other parameters: see Fig. 9.

waveguide modes turns from evanescent to propagating with respect to the y-direction. The grating efficiency is always greater than 0.6 (except for frequencies which are very close to the cutoff frequency of the fundamental mode of the rectangular waveguide) which means that more than 60% of the power of the incoming wave is absorbed by the waveguide array. As expected, the grating efficiency slowly tends to 0.7 at the upper end of the investigated frequency range which is just the ratio of the waveguide aperture and the area corresponding to one cell of the grating $(a \cdot b/\left((a+t) \cdot (b+t)\right))$.

It can be concluded from Figs. 14 and 15 that the average grating efficiency decreases for an increasing angle Θ. Furthermore the corresponding curves are characterized by rapid changes due to resonant effects. Nevertheless, even for the nearly grazing incident field with $\Theta = 85.5°$ an average grating efficiency of about 0.4 is observed in the considered frequency interval which still seems to be acceptable for the proposed absorber.

IV. Conclusions

The mode matching technique has been applied for the analysis of a two-dimensional array of rectangular waveguides which serves as a model for a HOM absorber. A detailed study of convergence has been carried out in order to demonstrate the accuracy of the presented method. Furthermore the validity of the results has been checked by comparing the excitation of the rectangular waveguide modes with corresponding numbers from MAFIA computations for the special case of normal incidence. The analysis of a grating with typical absorber dimensions has shown that the average grating efficiency is quite high. Although this quantity decreases as we approach the case of grazing incidence the overall absorption properties of such a grating seem to be acceptable.

Acknowledgement

The authors are indebted to many colleagues from the S-Band linear collider study group and the TESLA collaboration who contributed to these ideas.

References

[1] R. Brinkmann *et al.* (ed.), *Conceptual design of a 500 GeV e^+e^- linear collider with integrated X-ray laser facility*, DESY 1997-048, 1997.

[2] M. Dohlus, N. Holtkamp, A. Jöstingmeier, H. Hartwig and D. Trines, "Design of a HOM broadband absorber for TESLA", *Meeting note: 31 Linear collider project meeting at DESY*, 1998.

[3] M. Dohlus, N. Holtkamp and A. Jöstingmeier, "Design of a broadband absorber for $f >$ 100 GHz", *Meeting note: 26 Linear collider project meeting at DESY*, 1997.

[4] A. Wexler, "Solution of waveguide discontinuities by modal analysis", *IEEE Trans. Microwave Theory Tech.*, vol. MTT-15, pp. 508–517, 1967.

[5] P. H. Masterman and P. J. B. Clarricoats, "Computer field-matching solution of waveguide transverse discontinuities", *Proc. IEE*, vol. 118, pp. 51–63, 1971.

[6] T. Itoh (ed.), *Numerical Techniques for Microwave and Millimeter-Wave Passive Structures*, John Wiley & Sons, 1989.

[7] T. Weiland, "On the numerical solution of Maxwell's equations and applications in the field of accelerator physics", *Particle Accelerators*, vol. 15, pp. 245–292, 1984.

[8] The MAFIA collaboration, *User's Guide MAFIA Version 3.2,* CST GmbH, Lauteschlägerstr. 38, D64289 Darmstadt.

[9] R. F. Harrington, *Time-Harmonic Electromagnetic Fields*, McGraw-Hill, 1961.

[10] R. E. Collin, *Foundations for Microwave Engineering*, McGraw-Hill, 1966.

[11] J. van Bladel, *Electromagnetic Fields*, Springer Verlag, 1985.